Reproducibility of small Ge2C6H10O7-added MgB2 bulks fabricated by ex situ Spark Plasma Sintering used in compound bulk magnets with a trapped magnetic field above 5 T

Petre Badica, Gheorghe Aldica, Mihai Alexandru Grigoroscuta, Mihail Burdusel, Iuliana Pasuk, Dan Batalu, Kévin Berger, Anjela Koblischka-Veneva, Michael Rudolph Koblischka

SCIENTIFIC REPORTS
nature research

Check for updates

OPEN

Reproducibility of small $Ge_2C_6H_{10}O_7$-added MgB_2 bulks fabricated by ex situ Spark Plasma Sintering used in compound bulk magnets with a trapped magnetic field above 5 T

P. Badica[1]✉, G. Aldica[1], M. A. Grigoroscuta[1,2], M. Burdusel[1], I. Pasuk[1], D. Batalu[2,3], K. Berger[4], A. Koblischka-Veneva[5,6] & M. R. Koblischka[5,6]

Bulk discs (20 mm diameter and 4.3 mm thickness) of MgB_2 added with $Ge_2C_6H_{10}O_7$ were obtained by Spark Plasma Sintering. Six samples with composition $MgB_2(Ge_2C_6H_{10}O_7)_{0.0014}$ and one undoped sample were fabricated under similar conditions and were magnetically characterized in order to determine the scattering of properties and reproducibility. The main source of the scattering of the properties is the decomposition of the additive due to elimination of the organic part in gas form, which occurs stepwise with intensive vacuum drops at around ~ 560 and ~ 740 °C. A third drop, which is sometimes not well resolved being part of the second peak at 740 °C, occurs at ~ 820 °C. The critical temperature at the midpoint of the transition, T_c, shows only a relatively small variation between 37.4 and 38 K, and the irreversibility field at a low temperature of 5 K takes values between 8 and 10 T. The pinning force and pinning force related parameters do not correlate with the carbon substituting for boron in MgB_2 and suggest a synergetic influence of the microstructural details and carbon. Overall, despite the superconducting properties scattering, the samples are of high quality. Stacked into a column of six samples, they can trap at the center and on the surface of the column a magnetic field of 6.78 and 5.19 T at 12 K, 5.20 and 3.98 T at 20 K and 2.39, and 1.96 T at 30 K. These promising values, combined with facile fabrication of the samples with relatively high quality and reproducibility, show the feasibility of their use in building complex and large compound arrangements for bulk magnets and other applications.

MgB_2 is a lightweight practical superconductor (density 2.63 g/cm^3), hence, it is highly valuable in portable applications. MgB_2 is a superconductor free of expensive rare earth and precious elements. Considering these aspects, MgB_2 bulks are of much interest for use in superconducting magnets[1–24] and related applications. For the development of the applications mentioned, an enhancement of the superconducting functional parameters of MgB_2 such as the critical current density (J_c), the irreversibility fields (H_{irr}), and the trapped magnetic field (B_{tr}) is required. Routes for control and enhancement of the properties in MgB_2 are related to the use of additions, specifics of the processing technologies roughly classified as in situ and ex situ, and to the quality and features of the raw materials. In the in situ approach, the superconductor is fabricated by reacting Mg and B at

[1]National Institute of Materials Physics, Street Atomistilor 405A, 077125 Magurele, Romania. [2]University Politehnica of Bucharest, Splaiul Independentei 313, 060042 Bucharest, Romania. [3]Fileo Buildup SRL, Street Aleea Politehnicii 4, 060816 Bucharest, Romania. [4]Université de Lorraine, GREEN, 54000 Nancy, France. [5]Experimental Physics, Saarland University, P.O. Box 151150, 66041 Saarbrücken, Germany. [6]Superconducting Materials Laboratory, Department of Materials Science and Engineering, Shibaura Institute of Technology, Tokyo 135-8548, Japan. ✉email: badica2003@yahoo.com

temperatures of 650–900 °C, while in the ex situ method the MgB_2 compound is sintered at higher temperatures up to about 1,200 °C.

In our work we fabricated by ex situ spark plasma sintering (SPS) high density MgB_2 bulks, pristine and with different additives[25]. Processing conditions were optimized for samples of 2 cm in diameter, i.e. for relatively small ones. Noteworthy is that larger samples (up to 6 cm in diameter in our experiments) exhibit a lower density and less uniformity, hence, this is an undesirable situation since superconducting properties are suppressed.

SPS technique applies a pulsed current on a die system with punches loaded with the MgB_2 raw powder. The sample is subjected to uniaxial compression. Both, the current and the pressure on the sample facilitate consolidation processes. SPS has a high flexibility allowing high heating and cooling rates and it provides an excellent control of the processing parameters. Despite this, the fabrication of MgB_2 bulks has some general drawbacks:

(i) Superconducting materials including MgB_2 are very sensitive to external factors and to achieve a high production reproducibility is not trivial;
(ii) Bulks with complex shapes and large sizes are difficult to fabricate and the scaling process is challenging.

For the MgB_2 superconductor, the particular reasons are related to the highly volatile nature of Mg, the refractory character of B, the temperature behavior of the additives, the brittle and hard identity of MgB_2, and the complexity of the processes taking place during sintering, depending on the specifics of the technology. Search for solutions by proper understanding of the processes and their problems in certain conditions is essential for the assessment of the potential for industrial implementation of a given technology and material. An important question is the need of fabricating large-sized samples, e.g., for bulk magnet applications. Assembly of small samples into a desired complex arrangement or geometry instead of using a single large piece can be a simple and convenient solution, if the performance of the superconducting device composed of many elements is high and the fabrication costs are acceptable. The use of small pieces can also overcome the problem of building not only large, but also complex shapes that are otherwise difficult or impossible to fabricate. The addressed aspects are among the key priorities of the research in the applied superconductivity community and through the study proposed in this work, we provide several arguments in favor of small bulks and for their use in compound magnets and other applications.

Many additives introduced to MgB_2 that is fabricated by ex situ SPS improve the superconducting functional parameters[25]. Among them, the organometallic addition of Repagermanium ($Ge_2C_6H_{10}O_7$) greatly enhances the pinning force, leading to higher J_c and H_{irr}. However, its use is expected to pose extra difficulties associated with its decomposition and reaction with MgB_2 in the SPS processing. The thermal behavior of $Ge_2C_6H_{10}O_7$ and of MgB_2 added with $Ge_2C_6H_{10}O_7$ was investigated by DSC/DTA/TG/mass spectroscopy measurements and the results were previously reported in Refs.[26,27]. In this work, we explore the reproducibility details from the structural, magnetic and pinning force viewpoints, when samples with the starting composition $MgB_2(Ge_2C_6H_{10}O_7)_{0.0014}$ are processed under fixed, optimized SPS conditions and the initial sample weight is kept constant. As-fabricated samples are disc-shaped with a diameter of 2 cm and a thickness of ~ 4.3 mm. They are defined as 'small' bulks. Six samples with additive and one pristine sample are compared with each other. The scattering of the superconducting properties is revealed and discussed in detail. Overall, the sample quality is high and this promotes their use for applications. Considering that a higher volume of the superconductor should generate larger magnetic fields[6,16,20], we designed and performed an experiment to investigate the trapped field of all six added MgB_2 discs stacked together in a column of about 27 mm height. The measured values of the trapped magnetic field on the surface of the column are larger than 5 T at 12 K, and 4 T at 20 K. This compound device shows good thermal stability when the decrease rate of the DC applied magnetic field for excitation in the + 5 to − 5 T range is 0.01 T/min. Results infer that the small MgB_2 bulks added with $Ge_2C_6H_{10}O_7$, as individual pieces or combined into complex arrangements have potential for magnet and related applications: the fabrication of large MgB_2 samples is not mandatory and small, high quality bulk samples can be employed.

Methods

The raw materials (Alfa Aesar) were MgB_2 powder (99.5% metal basis), and $Ge_2C_6H_{10}O_7$ (Repagermanium, Ge-132) (99.7% purity). Powder mixtures of 3.564 g (3.5275 g of MgB_2 and 0.0365 g of Ge-132) were loaded into graphite dies. Dies were introduced in a SPS furnace produced by FCT Systeme GmbH, Germany (model HPD-5). Six samples with additions and one pristine sample were processed by SPS at 1,150 °C for 3 min and under a uniaxial maximum pressure of 95 MPa[28]. The initial vacuum pressure in the SPS furnace was about 40 Pa. The heating rate was 110 °C/min. The details of the sintered discs are presented in Table 1.

The apparent densities ρa^{SPS} (Table 1) of the SPSed discs were measured by the Archimedes method in toluene. The theoretical densities ρt^{SPS} of the composites were determined according to Ref.[29] considering the phase assembly. The samples are composed of MgB_2 (2.63 g/cm^2), MgO (3.58 g/cm^2), MgB_4 (2.49 g/cm^3), and Mg_2Ge (2.61 g/cm^2). The relative density is $R^{SPS} = \rho a^{SPS}/\rho t^{SPS} \times 100\%$.

X-ray diffraction (XRD) patterns were measured employing a Bruker AXS D8 Advance diffractometer ($Cu_{K\alpha}$ radiation). The weight fraction of the phases (Table 1) was extracted by Rietveld analysis (MAUD 2.31[30]). The lattice parameters, a and c of MgB_2, the crystallite size, and the residual strain for different phases were estimated (Table 1). The amount of carbon, y, substituting boron in the crystal lattice of MgB_2 ($Mg(B_{1-y}C_y)_2$) was calculated as a function of a (nm), $y = -21.9 \cdot a + 6.76$[31], using data from Refs.[32–34].

The displacement curves of the punches and the pressure variation in the furnace were registered by the SPS equipment during processing.

Samples were cut from the MgB_2 disks in the form of parallelepipeds ($\sim L \times l \times g = 1.5 \times 1.5 \times 0.5$ mm^3).

Sample	Lattice parameters of MgB_2		y	Phase content (wt%)/crystallite size (nm)				Strain in MgB_2 (%)	Apparent density ρa^{SPS} (g/cm^3)	$T_c^{midpoint}$ (K)
	a (Å)	c (Å)		MgB_2	MgB_4	MgO	Mg_2Ge			
I (pristine)	3.0836 ± 0.0003	3.5276 ± 0.0008	0.007 ± 0.001	78.6 ± 0.5/113 ± 3	13.3 ± 0.3/99 ± 3	8.1 ± 0.2/31 ± 1	–	0.14	2.51 ± 0.02	38.2
II	3.0812 ± 0.0007	3.5321 ± 0.0003	0.012 ± 0.002	73.2 ± 0.5/142 ± 2	16.1 ± 0.3/71 ± 3	10.0 ± 0.1/65 ± 1	0.70 ± 0.03/56 ± 5	0.15	2.57 ± 0.02	37.4
III	3.0824 ± 0.0008	3.5254 ± 0.0005	0.010 ± 0.002	73.5 ± 0.5/158 ± 4	16.1 ± 0.3/73 ± 1	9.7 ± 0.1/76 ± 2	0.70 ± 0.03/56 ± 5	0.14	2.55 ± 0.02	37.4
IV	3.0811 ± 0.0005	3.5260 ± 0.0004	0.012 ± 0.001	74.5 ± 0.5/154 ± 4	15.4 ± 0.3/71 ± 3	9.4 ± 0.1/74 ± 2	0.75 ± 0.03/60 ± 5	0.14	2.58 ± 0.02	37.4
V	3.0806 ± 0.0002	3.5248 ± 0.0009	0.013 ± 0.001	73.0 ± 0.5/158 ± 3	16.4 ± 0.3/72 ± 1	10.0 ± 0.1/72 ± 2	0.70 ± 0.03/61 ± 6	0.15	2.58 ± 0.01	37.5
VI	3.0801 ± 0.0006	3.5249 ± 0.0008	0.015 ± 0.001	72.6 ± 0.5/154 ± 3	16.6 ± 0.3/70 ± 2	10.0 ± 0.1/73 ± 2	0.75 ± 0.03/59 ± 3	0.14	2.57 ± 0.01	37.6
VII	3.0813 ± 0.0005	3.5254 ± 0.0008	0.012 ± 0.001	74.4 ± 0.5/149 ± 3	15.3 ± 0.3/73 ± 5	9.6 ± 0.2/75 ± 2	0.70 ± 0.10/57 ± 4	0.14	2.60 ± 0.01	37.4

Table 1. Samples, lattice parameters a and c, amount y of carbon substituting boron in MgB_2 ($Mg(B_{1-y}C_y)_2$), phase content, crystallite size, residual strain, apparent density, and midpoint critical temperature $T_c^{midpoint}$.

Magnetic hysteresis loops, $m(B)$, at different temperatures were measured employing a Vibrating Sample Magnetometer (VSM-9T, Cryogenic). The critical current density, J_c, was determined with the Bean formula for a plate-like geometry[35]:

$$J_c = 20 \cdot |m \uparrow - m \downarrow| / \{V \cdot l \cdot [1 - l/(3 \cdot L)]\}, \quad (1)$$

where m is the magnetic moment in emu for ascending and descending magnetic field, V is the sample volume in cm^3, and L, l are in cm.

The self-field J_{c0} (in A/cm^2) was estimated from the modified Bean relation, considering the descending branch of the hysteresis loop[36]:

$$J_c = 60 \cdot |m \downarrow| / (V \cdot l). \quad (2)$$

This approach is useful to avoid the complications with macro flux jumps that occur at low temperatures and with the estimation of $|m\uparrow - m\downarrow|$ in the classic Bean model. The irreversibility field $\mu_0 H_{irr}$ was established for a criterion of 100 A/cm^2.

The pinning force ($F_p = J_c \times \mu_0 \cdot H_{appl}$) was calculated. Fitting of the experimental data with the *universal scaling law*[37,38]

$$f_p = A \cdot h^p \cdot (1 - h)^q, \quad (3)$$

where $f_p = F_p/F_{p,max}$ with $F_{p,max}$ being the maximum pinning force, $h = H_{appl}/H_{irr}$, and A, p and q are fitting parameters, provides in the case of MgB_2[25] p and q values far away from the theoretical ones. From this reason we shall not present them here. Considering percolation aspects, Eisterer[39] defined the parameter $k_n = h_0/h(f_p/2)$. The values of $h_0 = h(f_p = 1)$ and k_n provide information on the vortex pinning mechanisms[38]. Theoretical values for Grain-Boundary Pinning (GBP) and Point Pinning (PP) are $h_0 = 0.2$, $k_n = 0.34$ and $h_0 = 0.33$, $k_n = 0.47$, respectively[38,39].

Trapped magnetic field experiments were performed by using a 5 T superconducting coil (Oxford Instruments) built in a low-loss cryostat. The room-temperature bore of the coil has a diameter of 75 mm and a cryocooler ARS-4K system is fitted inside it. The lowest temperature that can be used for the measurements is about 9 K. A bi-directional power supply for the superconducting coil (Oxford Instruments) enables a continuous sweep of the magnetic field with rates up to 2.4 T/min (40 mT/s). Hall probes with a linear signal and with a sensibility higher than 70 mV/T are of HHP-NP type from Arepoc s.r.o. (Slovakia). The size of the Hall sensor is $7 \times 5 \times 1$ mm^3 and the size of the active area is 0.35 mm^2. In our experiments we use simultaneously two sensors: one is placed inside the column made of 6 MgB_2 added discs, and the other one is located on the surface of the stacked column. The sample stage with the mounted samples is presented in Fig. 1a, c. The Hall probe 'at the center' corresponds to the situation of a pair-type magnet where each magnet is formed by three stacked discs of MgB_2. A copper ring (Fig. 1b) is fastened around the upper 3-samples stack to provide additional rigidity and to improve the thermal transfer during the cooling of the samples. For thermal purpose, copper foils are placed in between the 'pairs'. They also play the role of spacers for the introduction of the Hall probe. Two Cernox sensors, one on the cryocooler cold head and the second one on the opposite side of the sample holder measure the minimal T_{min} and maximal T_{max} temperatures. The temperature of the MgB_2 stacked column is taken as the average of the two temperatures. The difference between the two temperatures $\Delta T = T_{max} - T_{min}$ is 10, 6 and 4 K for a mean temperature of 12, 20 and 30 K, respectively. Samples are energized in the *field-cooling* process: in the normal state, e.g. at 40 K, a magnetic field of 5 T is applied, and the sample is cooled down to the desired temperature. Then, the applied magnetic field, B_{app}, is decreased with a fixed sweep rate towards − 5 T. The sweep rate is selected as high as possible, but so that the thermomagnetic instabilities (macro flux jumps) are avoided. The difference between the measured field, B_{meas}, and the applied field, B_{app}, defines the trapped magnetic field B_{tr}. In the literature[35], often the trapped magnetic field is taken for $B_{app} = 0$ T. Actually, this is the remnant trapped magnetic field $B_{rem} = B_{tr}$ (0 T) and considering the magnetic polarization $\mu_0 M$, the maximum trapped value is higher and it is obtained at negative values of the sweeping applied magnetic field B_{app}. We shall consider and use the notation, $B_{tr.max}$, for the maximum value of the trapped magnetic field. The local density of magnetic energy W is calculated as:

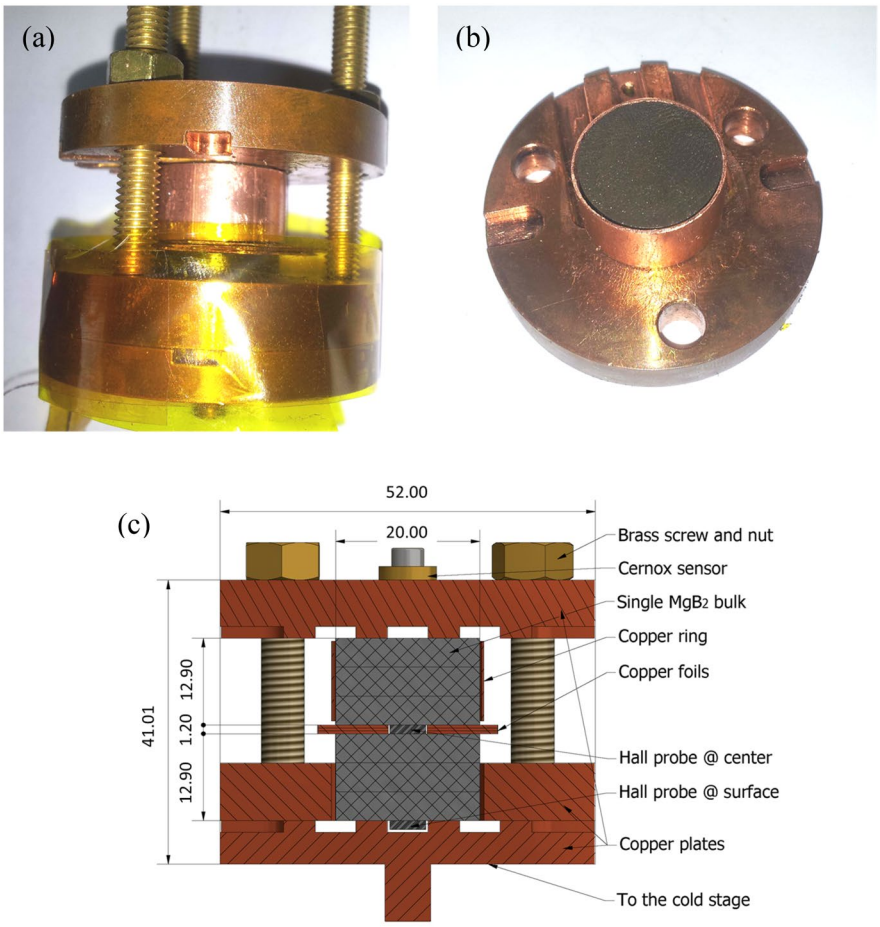

Figure 1. (**a**) Sample stage for trapped magnetic field measurement; (**b**) Copper ring with a diameter of 20 mm in which are introduced the MgB_2 superconducting discs for a rigid assembly into the compound column-magnet stack; (**c**) Schematic drawing (cross-section) of the six discs mounted in the sample holder. All dimensions are in mm.

$$W = B_{\text{meas}} \cdot H_{\text{app}}. \tag{4}$$

Results

Processing and evolution of structural details during SPS. The curves showing the relative contraction of the samples during SPS determined from the vertical displacement of the die punches as a function of processing time are presented in Fig. 2a. The curves for the samples II–VII with addition present some scattering, but the shape of the curves is found to be roughly similar. The shape of the curve of the pristine sample I is clearly different, showing a slower saturation on advanced stages of the SPS processing. The apparent density of the pristine sample I (2.51 g/cm^3, Table 1) is slightly lower than for the samples with additions II–VII (2.55–2.60 g/cm^3, Table 1). Results suggest that the additive has a strong influence on the densification processes during SPS, promoting a higher apparent density of the sintered bulk. The scattering of the apparent density versus theoretical density of added MgB_2 samples is $(2.60–2.55)/2.63 \times 100 = 1.9\%$. This value is appreciated as acceptably low considering that a relative density above 90% as for our samples from this work has a very low influence on the critical current density[28,40].

Scattering of the density and of the superconducting properties addressed in "Methods" are linked with reproducibility of the SPS processes, critical being those in which gas phases participate. Contribution is from Mg in the gas state and from the Ge-132 additive thermally decomposing with elimination of the organic component in the gas form. According to Mg-B phase diagrams from Ref.[41], under our SPS processing conditions, the presence of Mg in the gas state is expected. Mg occurs as the result of the decomposition reactions:

$$MgB_2 \rightarrow Mg + 2B, \tag{5}$$

$$2MgB_2 \rightarrow Mg + MgB_4. \tag{6}$$

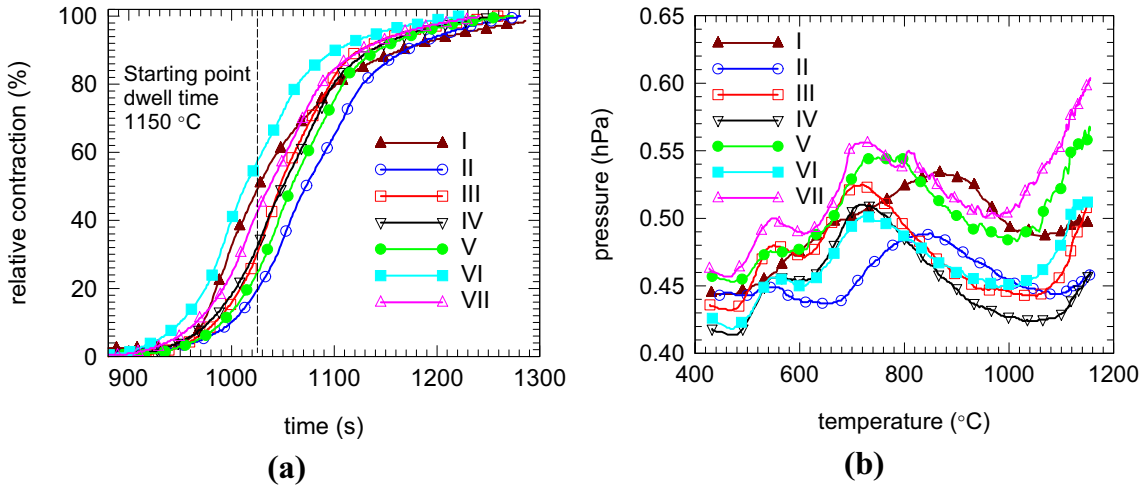

Figure 2. The evolution of the relative contraction with time (**a**), and the pressure in the SPS furnace as a function of temperature (**b**) for samples I–VII during the SPS processing.

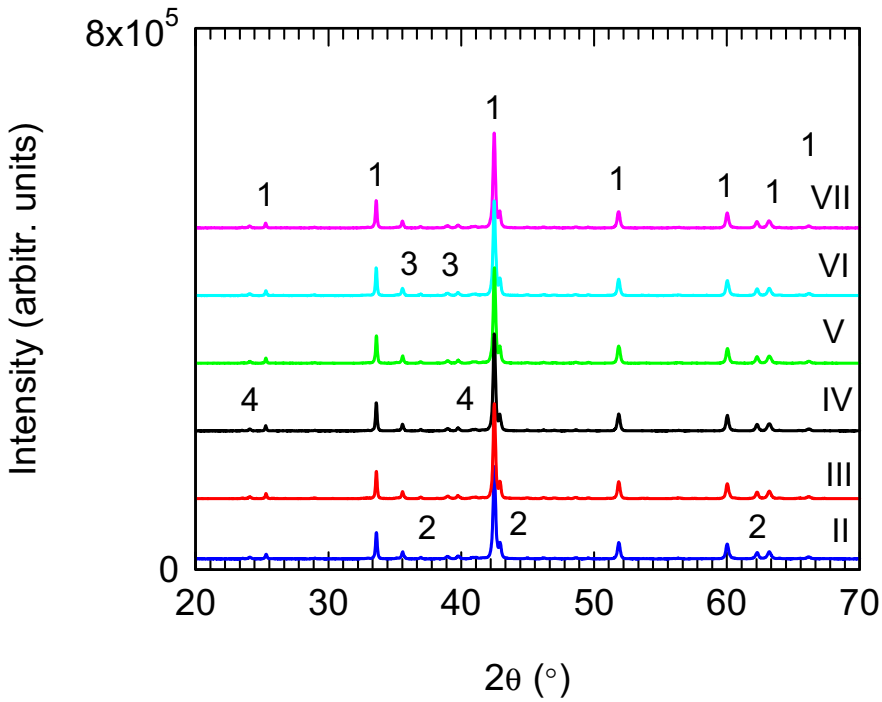

Figure 3. XRD patterns of samples "II–VII" (Table 1). Phases are 1-MgB_2 (ICDD 72-7019), 2-MgO (ICDD 35-0821), 3-MgB_4 (ICDD 73-1014), and 4-Mg_2Ge (ICDD 02-1135).

Free boron from (5) was not present in our XRD patterns. B-based phases in the Mg-B-O system from MgB_2 samples are observed by electron microscopy and due to their nanometer size, these are not detected by XRD. Reaction (6) is justified by the presence of MgB_4 phase in our XRD patterns (Fig. 3, Table 1).

The gas pressure in the SPS furnace during SPS processing has a complex behavior. For the samples with additions II–VII, intensive vacuum drops (or peaks of pressure-increase in the furnace in Fig. 2b) are observed at around ~ 560 and ~ 740 °C. A third peak that sometimes is not well resolved (being part of the second peak at 740 °C), occurs at ~ 820 °C. Its intensity is lower than for the peak at ~ 740 °C (an exception is seen for sample II). In the pristine sample, the first peak does not occur, the second one is very broad, and its maximum is found at ~ 840 °C. Therefore, the peaks at ~ 560 and 820 °C are ascribed to processes with gas formation. The first peak is generated mainly by decomposition of Ge-132 in the added samples, and the second is related with MgB_2 behavior since it occurs in the pristine sample. In addition, we note that in Ar atmosphere and for a heating rate of 10 °C/min, Ge-132, pristine or in a powder mixture with composition $(MgB_2)_{0.97}(Ge_2C_6H_{10}O_7)_{0.03}$,

starts decomposing at low temperatures ~ 215 °C[26,27]. In experiments from Ref.[27], the crystalline Ge and MgO were detected before formation of Mg_2Ge and MgB_4, when the temperature approaches the melting point of Ge (938 °C). This implies that the reaction (6) occurs at higher temperatures than reaction (5) and Mg as a product of (6) easily reacts with residual oxygen and forms MgO:

$$Mg + 1/2O_2 \rightarrow MgO. \quad (7)$$

The Ge-metal from the Ge-132 decomposition reacts with Mg from (5) and especially from (6) by the following reaction:

$$2Mg + Ge \rightarrow Mg_2Ge. \quad (8)$$

Carbon substitution for boron in the crystal lattice of MgB_2 was observed above 590 °C.

The results presented here cannot be directly applied to processes during SPS since in this case the atmosphere is vacuum, the heating rate is much higher (110 °C/min) and a uniaxial pressure is applied to the sample during SPS, but they are helpful to understand the reaction mechanisms.

For SPS conditions, the use of Ge-132 additive influences the reactions (5)–(7): the amount of MgB_2 in the pristine sample (78.6 wt%) is higher than in the samples with addition (72.6–74.5 wt%) and the difference (4.1–6 wt%) is larger than the amount of Mg_2Ge (0.7–0.75 wt%). Thus, the additive promotes the decomposition of MgB_2 and the reactions (5 + 7) and (6), but the features of these reactions comparative to pristine sample are modified. In support of this idea we also note that in the added samples II–VII the crystallite size of MgO (65–76 nm) is larger and the size of the MgB_4 grains is smaller (70–73 nm) than in the pristine sample (31 and 99 nm, Table 1). Moreover, the average crystallite size of MgB_2 in the added samples (146–158 nm) is larger than for the pristine sample (113 nm).

Another observation of interest is that in the samples with addition, above 1,100 °C, the vacuum in the SPS furnace shows the tendency for worsening (Fig. 2b). A possible decomposition reaction at high temperatures during SPS is:

$$MgB_4 \rightarrow Mg + 4B. \quad (9)$$

The additive is acting also as a source of carbon substituting boron in MgB_2. Possible mechanisms involved in this process might be similar to those for other organic type compounds[42] added to MgB_2, but more research is needed. In added samples the amount of C (0.010–0.015) is higher than in the pristine sample (0.007). The y_{Carbon} in the raw powder was 0.002. This value is lower than for the pristine sample I ($y = 0.007$). Data suggest that there is an intake of carbon from the graphite die used in the SPS processing. The scattering of y_{Carbon}-values in added samples is apparently high. Despite of this, the microstrain is not sensitive to the y-variation as one would expect, and it takes an approximately constant value of 0.14–0.15%. For samples with addition, no direct correlation was observed between the vacuum pressure behavior during SPS and the structural parameters scattering.

Critical current density, irreversibility field, and pinning force. A higher amount y of carbon in the samples with addition (Table 1), pushes the midpoint critical temperature $T_c^{midpoint}$ (37.4–37.6 K) to lower values than in the pristine sample (38.2 K) (Fig. 4a).

Although the decrease is not significant, only about 0.6–0.8 K, the carbon substitution for boron in MgB_2 and the changes in the composite microstructure of the added samples promote an increase of the critical current density J_c at high magnetic fields (Fig. 5). The microstructure was reported in Ref.[43]. Filamentary 1D nano grains with Ge and Mg ascribed to Mg_2Ge of 10–25 nm in length and 2–3 nm thickness were observed. Their size is comparable with coherence length of MgB_2, and, hence, they can play the role of efficient pinning centers. Also, the other secondary phases, MgO and MgB_4, form nano precipitates and can contribute pinning and J_c at high magnetic fields.

The enhancement of J_c at high magnetic fields is reflected by an increase of $\mu_0 H_{irr}$ at different temperatures (Fig. 4b) in the added samples (the exception from this behavior is sample II). At 5 K, the enhancement of $\mu_0 H_{irr}$ is up to 2 T when compared with the value for pristine sample I. Hence, the maximum enhancement, or the scattering of the irreversibility field in added samples represents about 25% of the $\mu_0 H_{irr}$ for the pristine sample.

A decrease of J_{c0} is observed for some of the added samples (e.g. for samples II and IV, Fig. 4c) and it does not correlate with the amount of carbon, y: usually, a higher y decreases J_{c0}, but this is not the case here. The samples V and VI with the highest values of y (Table 1) show larger and almost similar J_{c0} as compared to those for pristine sample I, respectively, in the entire studied temperature range (5–35 K). According to Birajdar and Eibl[44], 'colonies' of MgB_2 influence J_{c0}. Larger colonies promote a higher J_{c0}. The Ge-132 added samples[43] are composed of Ge poor and rich regions. The Ge-poor regions (5–100 μm) are compact and can be associated with 'colonies' embedded in a Ge-rich 'matrix'. In close vicinity of Ge, frequently oxygen was detected. Colonies can be considered relatively clean regions, while the matrix is relatively dirty. The Ge, O, and C distributions and phase assembly contribute to colonies features and J_{c0} scattering. Carbon in MgB_2 is present in the crystal lattice of MgB_2, as quantified by y_{Carbon}, and it can be also at grain boundaries. In the second case it is not detected by XRD. The J_{c0} variation is relatively low and it takes values at 5 K between 0.36 and 0.71 MA/cm^2.

The variation of J_{c0} among the samples influences the behavior of the quality product ($J_{c0} \cdot \mu_0 H_{irr}$) (Fig. 4d). The product for samples III, V and VII is higher, for sample VI is similar, and for samples II and IV is lower than the values for pristine sample I. The product is used in our comparative analysis to provide a quantitative measure of quality with information about the 'balance' between the superconducting parameters at low and high magnetic fields. The product has no practical or theoretical meaning.

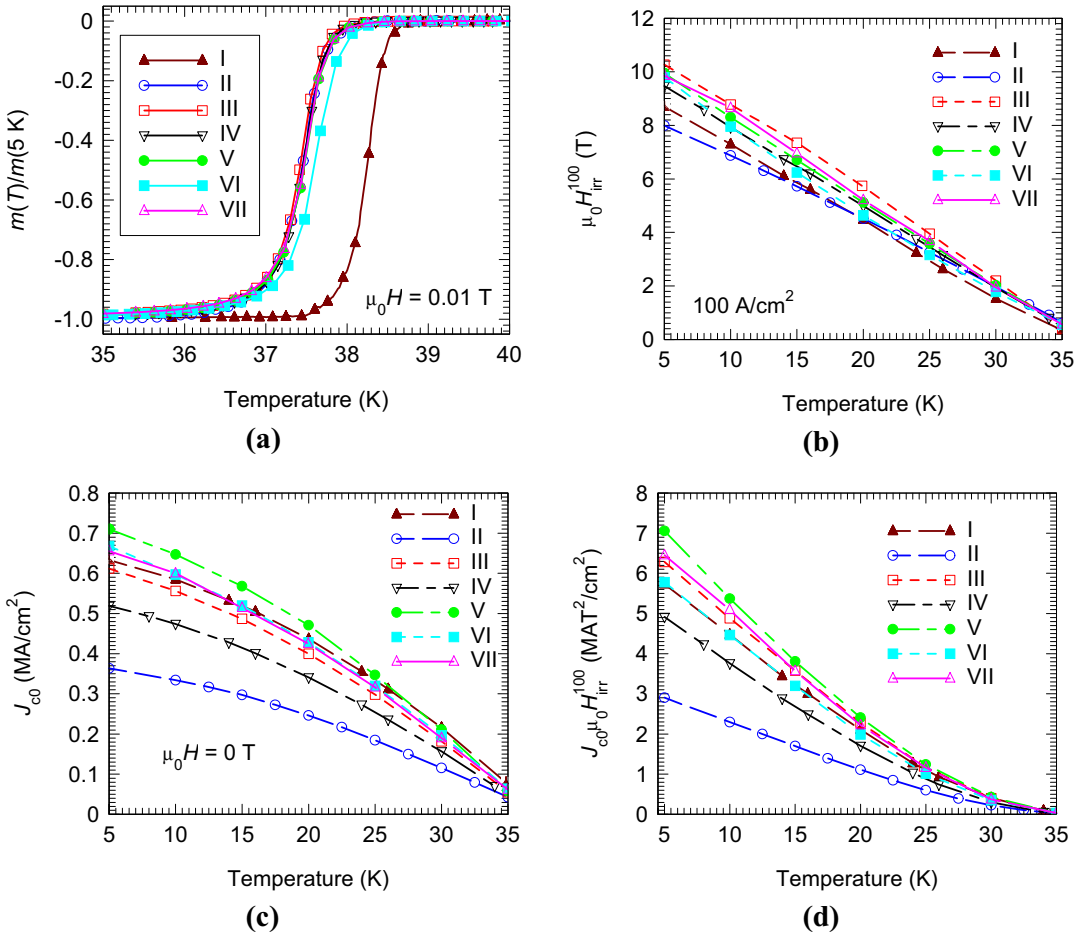

Figure 4. Temperature dependence of the reduced magnetization versus temperature measured in zero-field-cooling arrangement at 0.01 T (**a**), irreversibility field $\mu_0 H_{irr}$ (**b**), zero-field critical current density J_{c0} (**c**), and the product ($J_{c0} \times \mu_0 H_{irr}$) for pristine and added samples II–VII (**d**).

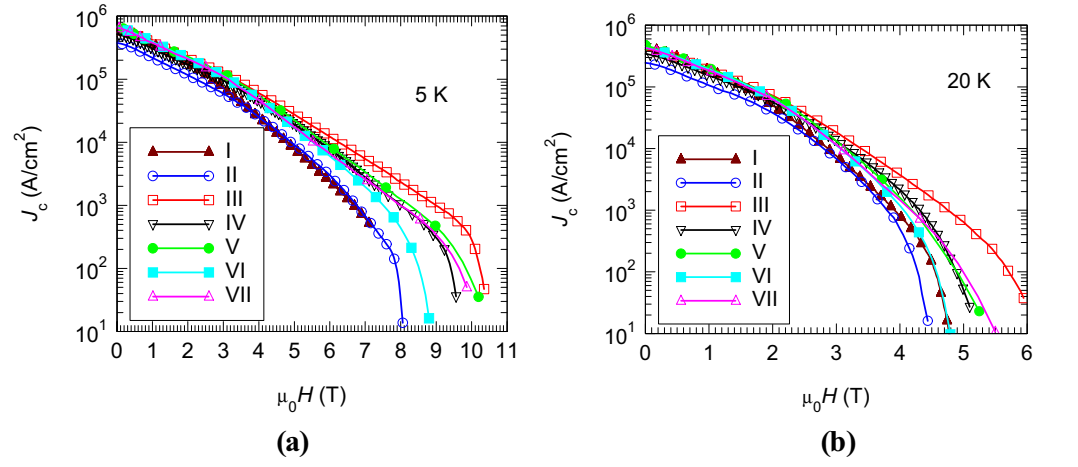

Figure 5. Critical current density versus applied magnetic field for samples I–VII at: (**a**) 5 K and (**b**) 20 K.

Results from the previous paragraphs suggest that scattering of J_c and H_{irr} in the added samples are induced not only by variation in the carbon amount y, but also by microstructural aspects of the composite samples. Both pinning and grain connectivity are influenced. For effective pinning one has to consider the nano precipitates of secondary phases, the density and type of interfaces and grain boundaries, the defects, and the micro strain. For a deeper understanding we shall look on the pinning force features.

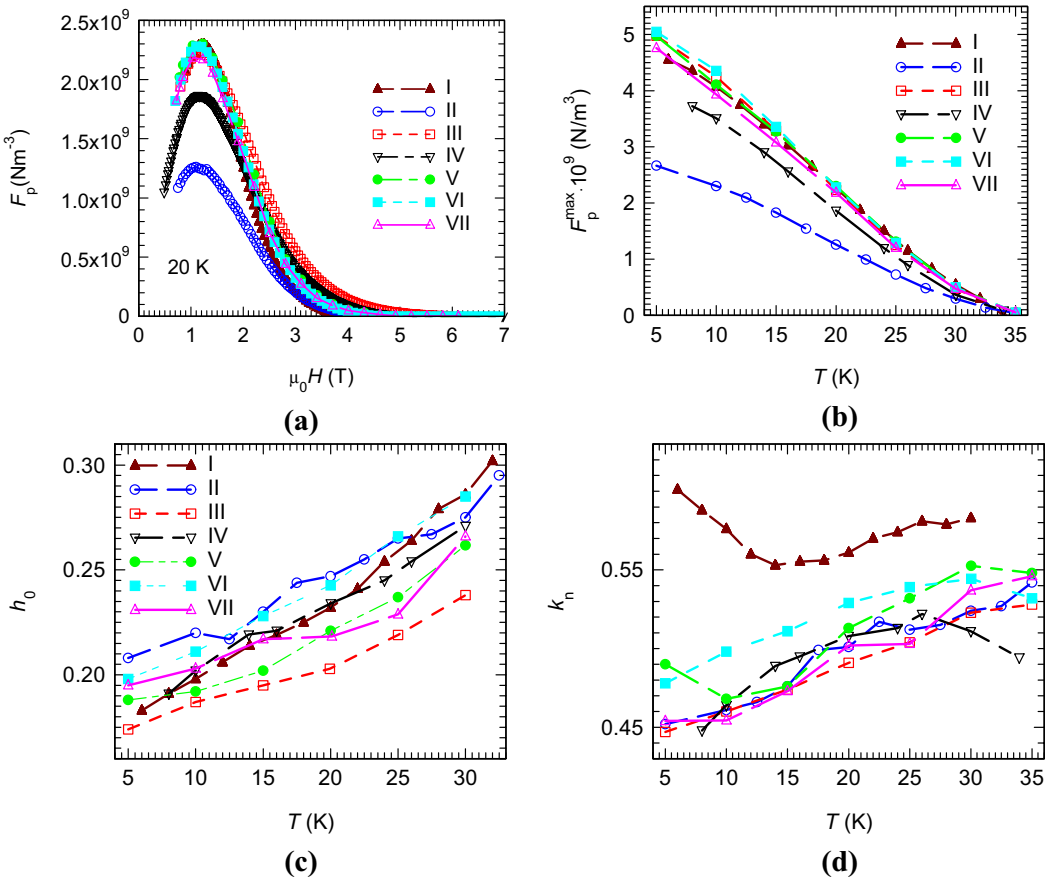

Figure 6. (**a**) The pinning force versus applied magnetic field at 20 K; (**b**) the maximum pinning force vs. temperature; (**c**) the reduced magnetic field for maximum pinning force as function of temperature; (**d**) pinning-force-related parameter k_n as a function of temperature. The samples notation is as given in Table 1 (I is the pristine sample and II–VII the added samples).

The added samples II–VII show a variation of the maximum pinning force at 20 K from 1.3×10^9 to 2.3×10^9 Nm^{-3} (Fig. 6a). The maximum pinning force for the pristine sample is, within the error range, similar to the values for the added samples III, V–VII, and it is higher than for samples II and IV at temperatures below 20 K (Fig. 6b). The pinning force parameters, h_0 and k_n as a function of temperature are presented in Figs. 6c, d.

At low temperatures, all samples show h_0 values close to 0.2, which is apparently suggesting a major grain boundary pinning (GBP) mechanism. At higher temperatures, h_0 increases to values close to 0.3 and indicates a stronger pinning mechanism on point defects (PP). The tendency of k_n to increase with temperature supports the results of h_0. Nevertheless, the values of k_n in the entire studied temperature range (5–35 K) are higher than 0.44, being above the theoretical values 0.34 for GPB and close or higher than 0.47 for PP. The contribution of GBP, that is more important at low temperatures, has a limited effect when compared to the predominant PP mechanism. We shall also observe that, as already reported in Ref.[25], a higher carbon amount y has a strong influence and pushes the curves of $h_0(T)$ and $k_n(T)$ to lower values, regardless of temperature (compare results for pristine sample I and added samples II–VII in Table 1 and in Figs. 6c, d), i.e., the GBP becomes stronger. On the other hand, the influence of nano precipitates and of other microstructural details (grain boundaries, defects, micro strain, others) on pinning force parameters cannot be neglected.

The scattering of h_0 for the samples with addition at different temperatures is between 0.027 and 0.047, while for k_n the range is between 0.03 and 0.052.

Trapped magnetic field. Trapped magnetic field B_{tr} at the center (B^c_{tr}) and on the surface (B^s_{tr}) of the compound magnet made of 6 discs is presented in Fig. 7. The trapped magnetic field curves without flux jumps were measured at 12, 20 and 30 K for the decrease rate of the DC applied magnetic field for excitation in the + 5 to − 5 T range of 0.01, 0.02, 0.1 and 0.5 T/min, respectively. The lower the working temperature of the compound magnet is, the lower the rate of applied magnetic field sweep without flux jumps should be.

In our work[10] we measured the MgB_2-NdFeB pair magnet (at the center) composed of a permanent magnet (thickness 8 mm, diameter 20 mm) placed below of a MgB_2 superconducting disc (thickness 3.5 mm, diameter 20 mm) fabricated by SPS. The trapped magnetic field attained 3.2 T at 12 K for a sweep rate of the DC applied magnetic field of 0.03 T/min. The NdFeB permanent magnet generates a field of about 0.5 T, while the remnant

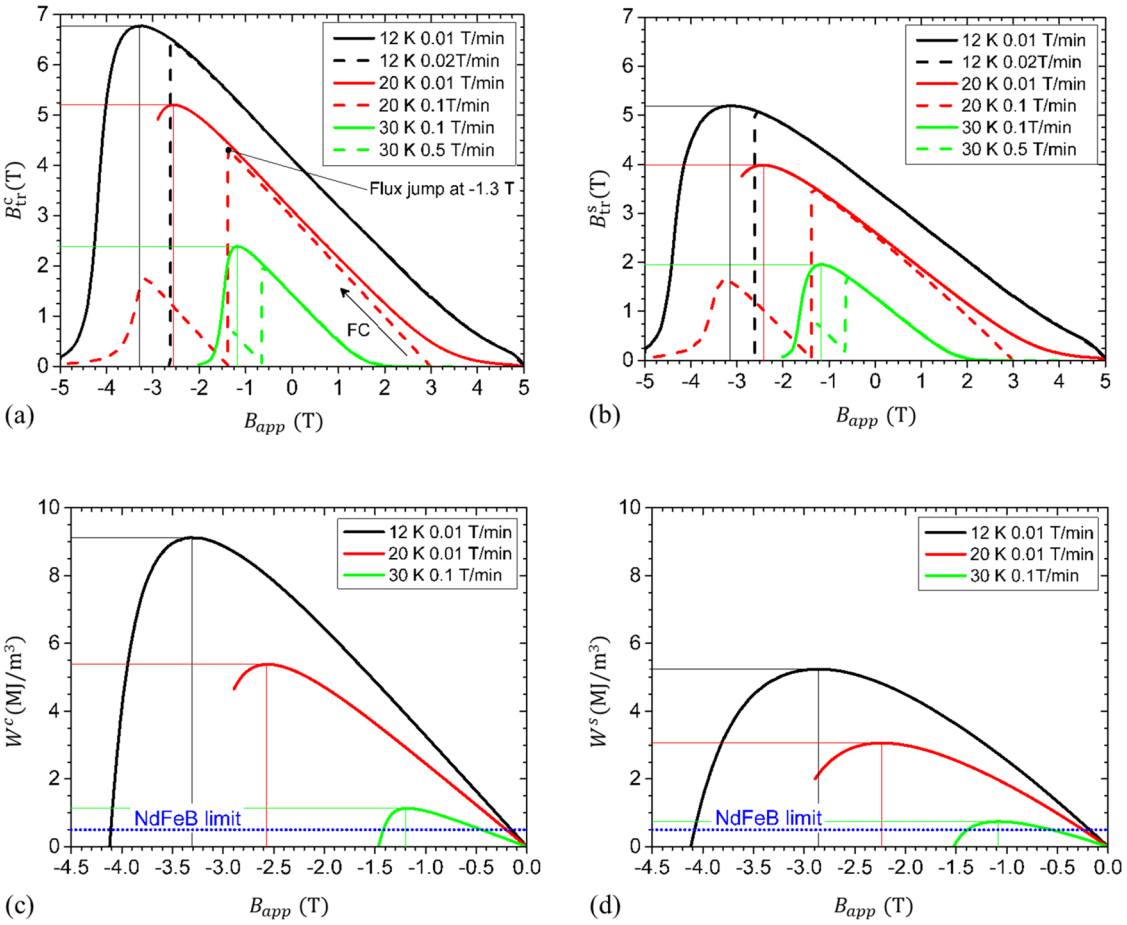

Figure 7. Trapped magnetic field at the center (**a**) and on the surface (**b**) of the magnet composed of 6 MgB_2 superconducting discs (samples II–VII, Table 1). The local density of magnetic energy at the center (**c**) and on the surface (**d**) is compared with the magnetic energy of a NdFeB conventional magnet.

trapped field $B_{rem} = B_{tr}(0\ T)$ of a MgB_2 disc is about 2.8 T. One observes that the remnant trapped field at the center and at the surface of the column is B^c_{rem} (12 K) = 4.1 T, B^s_{rem} (12 K) = 3.5 T (Fig. 7a, b), i.e., it is higher than for one disc (2.8 T), but it is about 4.1 and 4.8 times lower, respectively, than the multiple of six times (i.e. 16.8 T) of the remnant trapped field for one disc.

The maximum trapped magnetic field of the column at the center and on the surface show high values of 6.78 and 5.19 T at 12 K, 5.20 and 3.98 T at 20 K, and 2.39 and 1.96 T at 30 K. It is remarkable that at 20 K or at lower temperatures the obtained values exceed the application threshold value of 3 T[4]. The maximum trapped field on the surface of our compound magnet (5.19 T) is comparable with record high 5.4 T measured at 12 K in Ref.[6] on the surface of a single bulk sample (20 mm diameter and 8 mm height) and it is higher than 2.2 T measured at 7.5 K in Ref.[22] on the surface of a stack of five discs (32 mm diameter, 6 mm thickness).

The values of the maximum local magnetic energy measured at the center W^c and at the surface W^s of the compound magnet (Fig. 7c, d) are 2.23 and 1.5 at 30 K, 10.8 and 6.1 at 20 K, and 18.3 and 10.5 at 12 K times larger than the magnetic energy of the NdFeB magnet. The energy of the NdFeB magnet is an intrinsic property of the material and it is not influenced by size and shape.

Conclusion

Small spark plasma sintered discs of MgB_2 added with $Ge_2C_6H_{10}O_7$ were obtained for fixed SPS processing conditions and raw materials. They show good reproducibility of the density, structural and superconducting properties. A relatively large scattering was encountered for the irreversibility field suggesting that this parameter is among the most sensitive ones. The scattering of the properties is related to complex decomposition processes of MgB_2 and of the additive. Contribution arises from carbon substitution for boron in the crystal lattice of MgB_2, but also from microstructural details.

Six discs were stacked together in a column and measured for trapped magnetic field at the center and on the surface. The trapped magnetic fields at the center and on the surface were 6.78 and 5.19 T at 12 K, 5.20 and 3.98 T at 20 K, and 2.39 and 1.96 T at 30 K, when the decrease rate of the DC applied magnetic field for excitation in the + 5 to − 5 T range was 0.01 at 12 K, 0.01 at 20 K, and 0.1 T/min at 30 K. For the indicated rates, the curves of trapped magnetic field with applied magnetic field are free of flux jumps. Relevant for applications are the values of the trapped field measured on the surface of the compound magnet.

The results enable further studies and use of small MgB_2 superconducting samples in large and complex-shape compound magnets and other applications. Furthermore, it demonstrates the feasibility of compound magnets made of small and reproducible MgB_2 discs.

Received: 1 April 2020; Accepted: 1 June 2020
Published online: 29 June 2020

References

1. Viznichenko, R. V. *et al.* Temperature dependence of the trapped magnetic field in MgB_2 bulk superconductors. *Appl. Phys. Lett.* **83**, 4360–4362. https://doi.org/10.1063/1.1629148 (2003).
2. Perini, E. *et al.* Magnetic field trapping in MgB_2 bulks and inserts. *IEEE Trans. Appl. Supercond.* **21**, 2690–2693. https://doi.org/10.1109/TASC.2010.2086043 (2011).
3. Giunchi, G. MgB_2 superconductive inserts: Products between bulks and wires. *IEEE Trans. Appl. Supercond.* **21**, 12022666. https://doi.org/10.1109/TASC.2010.2092739 (2011).
4. Durrell, J. H. *et al.* A trapped field of > 3 T in bulk MgB_2 fabricated by uniaxial hot pressing. *Supercond. Sci. Technol.* **25**, 112002. https://doi.org/10.1088/0953-2048/25/11/112002 (2012).
5. Naito, T., Sasaki, T. & Fujishiro, H. Trapped magnetic field and vortex pinning properties of MgB_2 superconducting bulk fabricated by a capsule method. *Supercond. Sci. Technol.* **25**, 095012. https://doi.org/10.1088/0953-2048/25/9/095012 (2012).
6. Fuchs, G. *et al.* High trapped fields in bulk MgB_2 prepared by hot-pressing of ball-milled precursor powder. *Supercond. Sci. Technol.* **26**, 122002. https://doi.org/10.1088/0953-2048/26/12/122002 (2013).
7. Marignetti, F. *et al.* Use of MgB_2 superconductors for excitation field in synchronous machines—Part I: Bulk magnets. *IEEE Trans. Appl. Supercond.* **23**, 8002506. https://doi.org/10.1109/TASC.2013.2256354 (2013).
8. Marignetti, F. *et al.* Use of MgB_2 superconductors for excitation field in synchronous machines—Part II: Inserts. *IEEE Trans. Appl. Supercond.* **23**, 8002606. https://doi.org/10.1109/TASC.2013.2256355 (2013).
9. Sasaki, T., Naito, T. & Fujishiro, H. Trapped field of dense MgB_2 bulks fabricated under high pressure. *Phys. Proc.* **45**, 93–96. https://doi.org/10.1016/j.phpro.2013.04.060 (2013).
10. Aldica, G., Burdusel, M. & Badica, P. Trapped magnetic field in a (NdFeB)-MgB_2 pair-type bulk magnet. *Phys. C* **505**, 18–23. https://doi.org/10.1016/j.physc.2014.07.001 (2014).
11. Noudem, J. G. *et al.* Development in processing of MgB_2 cryo-magnet superconductors. *J. Appl. Phys.* **116**, 163916. https://doi.org/10.1063/1.4900725 (2014).
12. Muralidhar, M., Inoue, K., Koblischka, M. R., Tomita, M. & Murakami, M. Optimization of processing conditions towards high trapped fields. *J. Alloys Comp.* **608**, 102–109. https://doi.org/10.1016/j.jallcom.2014.04.017 (2014).
13. Yamamoto, A., Ishihara, A., Tomita, M. & Kishio, K. Permanent magnet with MgB_2 bulk superconductor. *Appl. Phys. Lett.* **105**, 132601. https://doi.org/10.1063/1.4890724 (2014).
14. Ujiie, T., Naito, T., Fujishiro, H., Albisetti, F. A. & Giunghi, G. Shielding and trapped field properties of large MgB_2 bulk. *Phys. Proc.* **58**, 306–309. https://doi.org/10.1016/j.phpro.2014.09.076 (2014).
15. Sugino, S., Yamamoto, A., Shimoyama, J. & Kishio, K. Enhanced trapped field in MgB_2 bulk magnets by tuning grain boundary pinning through milling. *Supercond. Sci. Technol.* **28**, 055016–055022. https://doi.org/10.1088/0953-2048/28/5/055016 (2015).
16. Zou, J. *et al.* Numerical modelling and comparison of MgB_2 bulks fabricated by HIP and infiltration growth. *Supercond. Sci. Technol.* **28**, 075009. https://doi.org/10.1088/0953-2048/28/7/075009 (2015).
17. Naito, T., Yoshida, T. & Fujishiro, H. Ti-doping effects on magnetic properties of dense MgB_2 bulk superconductors. *Supercond. Sci. Technol.* **28**, 095009. https://doi.org/10.1088/0953-2048/28/9/095009 (2015).
18. Naito, T., Ogino, A. & Fujishiro, H. Potential ability of 3 T-class trapped field on MgB_2 bulk surface synthesized by the infiltration-capsule method. *Supercond. Sci. Technol.* **29**, 115003. https://doi.org/10.1088/0953-2048/29/11/115003 (2016).
19. Bhagurkar, A. G. *et al.* A trapped magnetic field of 3 T in homogeneous, bulk MgB_2 superconductors fabricated by a modified precursor infiltration and growth process. *Supercond. Sci. Technol.* **29**, 035008. https://doi.org/10.1088/0953-2048/29/3/035008 (2016).
20. Berger, K. *et al.* High magnetic field generated by bulk MgB_2 prepared by spark plasma sintering. *IEEE Trans. Appl. Supercond.* **26**, 6801005. https://doi.org/10.1109/TASC.2016.2537143 (2016).
21. Ishihara, A., Akasaka, T., Tomita, M. & Kishio, K. Superior homogeneity of trapped magnetic field in superconducting MgB_2 bulk magnets. *Supercond. Sci. Technol.* **30**, 035006. https://doi.org/10.1088/1361-6668/30/3/035006 (2017).
22. Bhagurkar, A. G. *et al.* High trapped fields in C-doped MgB_2 bulk superconductors fabricated by infiltration and growth. *Sci. Rep.* **8**, 13320. https://doi.org/10.1038/s41598-018-31416-3 (2018).
23. Prikhna, T. *et al.* Pinning and trapped field in MgB_2- and MT-YBaCuO bulk superconductors manufactured under pressure. *J. Phys. Conf. Series* **695**, 012001. https://doi.org/10.1088/1742-6596/695/1/012001 (2016).
24. Masson, P., Leveque, J., Netter, D. & Rezzoug, A. Experimental study of a new kind of superconducting inductor. *IEEE Trans. Appl. Supercond.* **13**, 2239–2242. https://doi.org/10.1109/TASC.2003.813055 (2003).
25. Badica, P., Aldica, G., Ionescu, A. M., Burdusel, M. & Batalu, D. The influence of different additives on MgB_2 superconductor obtained by ex situ spark plasma sintering: Pinning force aspects. In *Correlated Functional Oxides* (eds Nishikawa, H. *et al.*) 75–116 (Springer, New York, 2017). https://doi.org/10.1007/978-3-319-43779-8_4 **(ISBN 978-3-319-43777-4)**.
26. Batalu, D. *et al.* Thermal analysis of repa-germanium (Ge-132). *Thermochim. Acta* **644**, 20–27. https://doi.org/10.1016/j.tca.2016.10.005 (2016).
27. Aldica, G. *et al.* Thermal analysis on $C_6H_{10}Ge_2O_7$-doped MgB_2. *J. Therm. Anal. Calorim.* **127**, 173–179. https://doi.org/10.1007/s10973-016-5877-9 (2017).
28. Aldica, G. *et al.* Spark plasma sintering of MgB_2 in the two-temperature route. *Phys. C* **477**, 43–50. https://doi.org/10.1016/j.physc.2012.01.023 (2012).
29. Marks, G. W. & Monson, L. A. Effect of certain group IV oxides on dielectric constant and dissipation factor of barium titanate. *Ind. Eng. Chem.* **47**, 1611–1620. https://doi.org/10.1021/ie50548a044 (1955).
30. Lutterotti, L. Total pattern fitting for the combined size-strain-stress-texture determination in thin film diffraction. *Nucl. Inst. Methods Phys. Res. B* **268**, 334–340. https://doi.org/10.1016/j.nimb.2009.09.053 (2010).
31. Aldica, G. *et al.* Dwell time influence on spark plasma-sintered MgB_2. *J. Supercond. Nov. Mag.* **31**, 317–325. https://doi.org/10.1007/s10948-017-4236-9 (2018).
32. Avdeev, M., Jorgensen, J. D., Ribeiro, R. A., Budko, S. L. & Canfield, P. C. Crystal chemistry of carbon-substituted MgB_2. *Phys. C* **387**, 301–306. https://doi.org/10.1016/S0921-4534(03)00722-6 (2003).
33. Lee, S., Masui, T., Yamamoto, A., Uchiyama, H. & Tajima, S. Crystal growth of C-doped MgB_2 superconductors: Accidental doping and inhomogeneity. *Phys. C* **412–414**, 31–35. https://doi.org/10.1016/j.physc.2004.01.036 (2004).
34. Dou, S. X. *et al.* Mechanism of enhancement in electromagnetic properties of MgB_2 by nano SiC doping. *Phys. Rev. Lett.* **98**, 097002. https://doi.org/10.1103/PhysRevLett.98.097002 (2007).
35. Bean, C. P. Magnetization of hard superconductors. *Phys. Rev. Lett.* **8**, 250–253. https://doi.org/10.1103/PhysRevLett.8.250 (1962).

36. Miu, L. *et al.* Improvement of the critical current density of spark plasma sintered MgB_2 by C_{60} addition. *Supercond. Sci. Technol.* **23**, 095002. https://doi.org/10.1088/0953-2048/23/9/095002 (2010).
37. Fietz, W. A. & Webb, W. W. Hysteresis in superconducting alloys—temperature and field dependence of dislocation pinning in niobium alloys. *Phys. Rev. B* **178**, 657–667. https://doi.org/10.1103/PhysRev.178.657 (1969).
38. Dew-Hughes, D. Flux pinning mechanisms in type II superconductors. *Philos. Mag. J. Theor. Exp. Appl. Phys.* **3**, 293–305. https://doi.org/10.1080/14786439808206556 (1974).
39. Eisterer, M. Calculation of the volume pinning force in MgB_2 superconductors. *Phys. Rev. B* **77**, 144524. https://doi.org/10.1103/PhysRevB.77.144524 (2008).
40. Dancer, C. E. J. *et al.* Fabrication and properties of dense ex situ magnesium diboride bulk material synthesized using spark plasma sintering. *Supercond. Sci. Technol.* **22**, 095003. https://doi.org/10.1088/0953-2048/22/9/095003 (2009).
41. Xi, X. X. *et al.* Deposition and properties of superconducting MgB_2 thin films. *J. Supercond.* **16**, 801–806. https://doi.org/10.1023/A:1026294632677 (2003).
42. Cai, Q., Ma, Z., Liu, Y. & Yu, L. Enhancement of critical current density in glycine-doped MgB_2 bulks. *Mater. Chem. Phys.* **136**, 778–782. https://doi.org/10.1016/j.matchemphys.2012.07.056 (2012).
43. Batalu, D. *et al.* High magnetic field enhancement of the critical current density by Ge, GeO_2 and $Ge_2C_6H_{10}O_7$ additions to MgB_2. *Scr. Mater.* **82**, 61–64. https://doi.org/10.1016/j.scriptamat.2014.03.024 (2014).
44. Birajdar, B. & Eibl, O. Microstructure-critical current density model for MgB_2 wires and tapes. *J. Appl. Phys.* **105**, 033903. https://doi.org/10.1063/1.3068361 (2009).

Acknowledgements

This work was supported by UEFISCDI Romania through Core Program PN19-03 (contract no. 21N/08.02.2019), the projects POC 37_697 no. 28/01.09.2016 REBMAT and PFE 12, and it is part of the SUPERFOAM international project funded by ANR and DFG under the references ANR-17-CE05-0030 and DFG-ANR Ko2323-10, respectively. D. B. acknowledges support from University POLITEHNICA of Bucharest (UPB), through the "Excellence Research Grants" Program, UPB—GEX, No. 51/2016, Code 300, NEWADD.

Author contributions

Conceptualization P.B. and K.B.; methodology, P.B., G.A., M.A.G., M.B., I.P., D.B., K.B., A.K-V, M.R.K.; validation, P.B., G.A., and I.P.; formal analysis, P.B., G.A., M.A.G., M.B., I.P., D.B., K.B., A.K-V, M.R.K.; investigation, P.B., G.A., M.A.G., M.B., I.P., D.B., K.B., A.K-V, M.R.K.; resources, P.B. and M.R.K.; writing—original draft preparation, P.B.; writing—review and editing, P.B., K.B., D.B., and M.R.K.; visualization, M.A.G. and P.B.; supervision, P.B.; project administration, P.B., K.B., and M.R.K.; funding acquisition, P.B., K.B., and M.R.K.

Competing interests

The authors declare no competing interests.

Additional information

Correspondence and requests for materials should be addressed to P.B.

Reprints and permissions information is available at www.nature.com/reprints.

Publisher's note Springer Nature remains neutral with regard to jurisdictional claims in published maps and institutional affiliations.